ISSN 0021-3640, JETP Letters, 2023, Vol. 117, No. 11, pp. 827–833. © The Author(s), 2023. This article is an open access publication.
Russian Text © The Author(s), 2023, published in Pis'ma v Zhurnal Eksperimental'noi i Teoreticheskoi Fiziki, 2023, Vol. 117, No. 11, pp. 832–839.

CONDENSED MATTER

Inverse Faraday Effect in Superconductors with a Finite Gap in the Excitation Spectrum

A. V. Putilov[a,*], S. V. Mironov[a], A. S. Mel'nikov[a, b], and A. A. Bespalov[a]

[a] *Institute for Physics of Microstructures, Russian Academy of Sciences, Nizhny Novgorod, 603950 Russia*

[b] *Moscow Institute of Physics and Technology (National Research University), Dolgoprudnyi, Moscow region, 141701 Russia*

**e-mail: alputilov@ipmras.ru*

Received March 30, 2023; revised April 17, 2023; accepted April 17, 2023

The inverse Faraday effect (generation of a time-independent magnetic moment under the action of a circularly polarized electromagnetic wave) in mesoscopic superconducting samples with a finite gap in the excitation spectrum is analytically described. Within the modified time-dependent Ginzburg–Landau theory (Kramer–Watts-Tobin equations) for thin superconducting disks, it is shown that the temperature dependence of the optically induced magnetic moment is nonmonotonic in a wide range of parameters and contains a maximum. This maximum is due to the dephasing between the spatial oscillations of the magnitude and the phase of the order parameter, which arises with a decrease in the temperature and, correspondingly, in the characteristic relaxation time of perturbations in the superconducting condensate.

DOI: 10.1134/S0021364023601239

The study of the mechanisms allowing one to control the magnetic states in superconductors using electromagnetic radiation is a rapidly developing field of condensed matter physics, which is motivated by the prospects for their applications in quantum computing devices [1, 2], elements of superconducting spintronics [3, 4], and dynamically tunable Josephson systems [5–8]. The key parameter that determines the character of the radiation impact on superconductors is the ratio between the photon energy and the size of the gap in the excitation spectrum of the superconductor. For optical radiation, this ratio is much larger than unity; therefore, the dominant mechanism of the radiation impact on a superconductor is the creation of quasiparticles, which can lead either to sample heating and suppression of superconductivity or to stimulation of superconductivity caused by an increase in the superconducting gap because of the generation of nonequilibrium quasiparticles [9–12]. In recent experiments, it was demonstrated that local heating of a superconductor by a focused laser beam makes it possible to control the position of single Abrikosov magnetic vortices [13], which provides the possibility of creating Josephson junctions with a tunable current–phase relation [5].

At the same time, for radiation with a photon energy less than the superconducting gap, the effects that depend not only on the photon energy and their flux density but also on the electromagnetic wave polarization become significant. Specifically, in a series of works [14–17], it was shown that circularly polarized infrared radiation incident on a superconducting sample can induce a magnetic moment with a nonzero time-averaged magnitude and with the direction determined by the incident wave polarization. This phenomenon called the inverse Faraday effect was first predicted for materials without absorption by L.P. Pitaevskii [18] and was observed experimentally in ferromagnetic insulators [19–22] and then in conducting materials [23, 24] (theoretical approaches to the description of the inverse Faraday effect in normal metals and semiconductors were developed in [25–33]). At the same time, the use of ultrashort laser pulses makes it possible to induce and control oscillations of the magnetic moment in a sample with a period on the order of several femtoseconds and a decay time on the order of a picosecond [22]. In fact, the impact of a circularly polarized wave on a medium is similar to the effect of a static magnetic field inducing the polarization of electron spins and the orbital diamagnetic response. In this context, the study of the inverse Faraday effect in superconducting systems is of particular interest, since diamagnetic superconducting currents induced by a laser pulse under certain conditions can exist indefinitely after the end of the pulse. In particular, if the magnitude of the optically induced magnetic moment is sufficient to generate an Abrikosov vortex or a state with nonzero vorticity in a multiply connected superconductor, then the resulting magnetic states are topologically protected and are not destroyed when the radiation is switched off [16].

The simplest description of the inverse Faraday effect in superconductors can be developed within the time-dependent Ginzburg–Landau theory [14]. In this case, the effect is primarily due to the electron–hole asymmetry in superconductors, which leads to the presence of the imaginary part of the relaxation constant in the Ginzburg–Landau equation and, as a consequence, to oscillations in the magnitude of the order parameter under the action of the electromagnetic wave. The theory developed in [14–17] makes it possible to analyze the frequency dependences of the optically induced magnetic moment and describe the formation of topologically protected magnetic states in multiply connected samples, but its applicability is significantly limited by the case of gapless superconductors and a narrow temperature range near the superconducting transition temperature.

At the same time, it is well known that the range of applicability of the time-dependent Ginzburg–Landau theory can be significantly expanded within the Kramer–Watts-Tobin approach [34–38], which takes into account the finite superconducting gap in the presence of a sufficiently strong electron–phonon coupling. In this paper, the theory of the inverse Faraday effect is generalized within this approach for the case of finite-gap superconductors, which makes it possible to analyze the temperature and frequency dependences of the optically induced magnetic moment in a wide range of system parameters. In particular, it is shown that, in a wide range of radiation frequencies, the temperature dependence of the magnetic moment M is nonmonotonic and has a maximum determined by a change in the ratio between the radiation frequency and the characteristic inverse relaxation time of the magnitude of the order parameter, which depends on the time. Although this phenomenon is also revealed in the case of gapless superconductivity (see [14]), it is important to take into account the finite superconducting gap because it leads to a shift of the maximum of the magnetic moment M down in temperature and, thus, makes it possible to specify the most realistic conditions for the experimental observation of the inverse Faraday effect.

As a model object, we consider a thin superconducting disk of the thickness L with an arbitrary ratio between the radius R and the superconducting coherence length ξ. We assume that a circularly polarized plane electromagnetic wave with a frequency ω and a wave vector $\mathbf{k}$ perpendicular to the disk surface is incident on the disk (Fig. 1). To describe the electromagnetic wave, we use the vector potential in the gauge $\mathbf{A} = \mathrm{Re}\tilde{\mathbf{A}} = (cE_0/\omega)\mathrm{Re}\left[\left(\mathbf{e}_y - i\mathbf{e}_x\right)e^{-i\omega t - ikz}\right]$, where $k = \omega/c$ is the magnitude of the wave vector and E_0 is the amplitude of the electric field inside the superconductor. The relation between this field and the electric field of the incident electromagnetic wave E_{ext} significantly depends on the shape of the disk and is determined by the depolarization effects. To estimate this relation, we replace the superconducting disk with an ellipsoid with semiaxes R, R, and $L/2$ and use the solution of the standard depolarization problem [39], which gives

$$\tilde{\mathbf{A}} = \frac{\tilde{\mathbf{A}}_{\mathrm{ext}}}{1 + (\pi/8)(L/R)[\epsilon(\omega) - 1]}, \qquad (1)$$

where $\epsilon(\omega)$ is the permittivity of the metal, which can be calculated under the assumption that the contributions from normal and superconducting electrons are additive. In the limit of the local relation between the current and the vector potential for the superconducting condensate under the assumption $\tau_{\mathrm{tr}} \ll 1/\omega$, where τ_{tr} is the characteristic impurity scattering time, the expression for $\epsilon(\omega)$ at temperatures below the superconducting transition temperature T_c has the form

$$\epsilon(\omega) = 1 - \frac{2\pi^2}{7\zeta(3)}\frac{T_c\tau_{\mathrm{tr}}}{\hbar}\frac{\omega_p^2\varepsilon}{\omega^2} + i\frac{\omega_p^2\tau_{\mathrm{tr}}}{\omega}, \qquad (2)$$

where the second term corresponds to the contribution from superconducting electrons [40], the third term corresponds to the contribution from normal electrons, $\omega_p^2 = 4\pi n_0 e^2/m$ is the square of the plasma frequency in metal, n_0 is the total electron density, $\varepsilon = 1 - T/T_c$, and $\zeta(3) \approx 1.2$ is the Riemann zeta function. The type of dependence $\epsilon(\omega)$ and, respectively, the linear relation between $\tilde{\mathbf{A}}_{\mathrm{ext}}$ and $\tilde{\mathbf{A}}$ are determined by the material and geometric parameters of the sample. We note that the permittivity at $\omega \gg T_c\varepsilon$ is determined mainly by normal electrons, and its temperature dependence can be neglected. In the opposite limit ($\omega \ll T_c\varepsilon$), the main contribution to the depolarizing factor comes from superconducting electrons. In this case, there is a resonant enhancement of the acting electromagnetic field at the frequency $\omega^* \sim \omega_p\sqrt{(L/R)\varepsilon\tau_{\mathrm{tr}}T_c/\hbar}$ and the corresponding enhancement of the magnetic moment. In what follows, we focus on the dependence of the magnetic moment of the disk on the acting electromagnetic field. Under the assumption that the geometric dimensions of the disk are much smaller than the London penetration depth λ, electromagnetic wavelength $2\pi c/\omega$, and skin layer depth $\delta \sim c/(\omega_p\sqrt{\omega\tau_{\mathrm{tr}}})$, the amplitude of the electromagnetic wave in the disk is given by Eq. (1) and is independent of the spatial coordinates.

To describe the dynamics of the order parameter, we use the Kramer–Watts-Tobin equation [38], where the imaginary part of the relaxation constant is intro-

duced in order to phenomenologically describe the electron–hole asymmetry in the density of states:

$$\frac{\Gamma(u+i\gamma)}{\sqrt{\Gamma^2+|\psi|^2}}\left(\psi_t+\frac{1}{2\Gamma^2}\psi\frac{\partial|\psi^2|}{\partial t}\right)$$
$$-\xi_0^2\alpha_0\left(i\nabla-\frac{\mathbf{A}}{\Phi_0}\right)^2\psi-\alpha_0\varepsilon\psi+b|\psi^2|\psi=0. \quad (3)$$

Here, $\alpha_0\varepsilon$ and b are the conventional parameters of the Ginzburg–Landau theory, $\Phi_0=\pi\hbar c/e$ is a magnetic flux quantum ($e>0$), ξ_0 is the coherence length interpolated to zero temperature, and $u=\hbar\pi\alpha_0/(8T_c)$. Equation (3) differs from the time-dependent Ginzburg–Landau equation in the additional parameter $\Gamma=\hbar\tau_{ph}^{-1}/2$ related to the inelastic electron–phonon relaxation time τ_{ph} and in the imaginary part of the relaxation constant γ, which has a relative order $\gamma/u\propto T_c/E_F$. For low-temperature superconductors and a number of high-temperature ones, $T_c/E_F\ll 1$, but the ratio T_c/E_F may be not too small for some high-temperature superconductors.

Although Eq. (3) is valid in a narrow region near the superconducting transition temperature, which is determined by the condition $\varepsilon\ll\Gamma/\Delta_0$ (where $\Delta_0=\sqrt{\alpha_0/b}$ is the order parameter interpolated to zero temperature), this constraint is less stringent than the limit of applicability of the time-dependent Ginzburg–Landau theory [38] $\varepsilon\ll(\Gamma/\Delta_0)^2$. Thus, the use of Eq. (3) makes it possible to generalize the results of [14] to the temperature range of $0\ll\varepsilon\ll\Gamma/\Delta_0$. Note that Eq. (3) correctly describes the dynamics of the order parameter at frequencies $\omega\ll\tau_{ph}^{-1}$ [40].

For simplicity, we disregard the electrochemical potential in Eq. (3), thus neglecting the processes of conversion between the superconducting and normal currents. These processes take place on a scale $l_e\sim\xi(T)(1+\psi_0^2/\Gamma^2)^{1/2}$, where $\psi_0=\sqrt{\alpha_0\varepsilon/b}$ is the equilibrium magnitude of the order parameter and $\xi=\xi_0/\sqrt{\varepsilon}$. Such approximation is valid when $l_e\gg\min(R,l_\omega)$, where l_ω is the characteristic length of perturbations of the order parameter under the effect of the electromagnetic wave. The scale l_ω is determined by the solution of Eq. (3) and, as shown below, is $l_\omega=\xi_0(1+\psi_0^2/\Gamma^2)^{1/4}/\sqrt{\omega\tau_0}$, $\tau_0=u/\alpha_0$. In the case $\psi_0\ll\Gamma$, the conversion scale l_e is comparable with the coherence length ξ, so that the region of applicability for the used approximation is determined by the condition $\min\left[R/\xi,\sqrt{\varepsilon/(\omega\tau_0)}\right]\ll 1$. On the other hand, in the case of well-developed superconductivity $\psi_0\gg\Gamma$, the expression for the conversion scale takes the form $l_e\sim\xi\psi_0/\Gamma$, which makes it possible to consider a wider temperature range near the critical temperature than that in [14], as well as large radii of superconducting disks. In this case, the limit on the possible R and ω values in the calculation of the inverse Faraday effect takes the form $\min\left[R\Gamma/(\xi\psi_0),\sqrt{\psi_0\varepsilon/(\Gamma\omega\tau_0)}\right]\ll 1$.

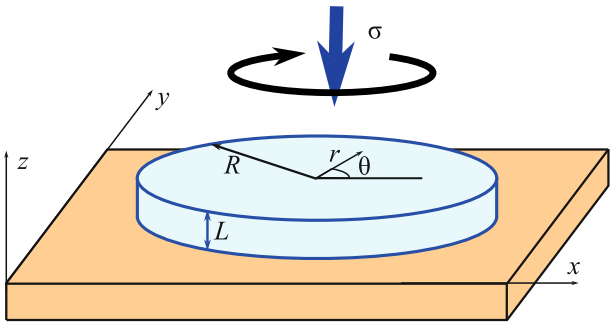

Fig. 1. (Color online) Schematic representation of the superconducting disk of the radius R and the thickness L exposed to the electromagnetic wave with the circular polarization σ. The figure also shows the Cartesian and polar coordinate systems used in the calculations.

Further, we solve a time-dependent problem using the perturbation theory, in which the small parameters are the amplitude of the incident electromagnetic wave and the parameter γ/u. The amplitude of the incident electromagnetic wave is treated as small if the induced perturbation of the order parameter is much less than the magnitude of the order parameter in the absence of the wave. We assume that the zero-order solution of Eq. (3) is a uniform static order parameter whose amplitude ψ_0 is temperature-dependent and the phase is assumed to be zero for definiteness. For further calculations, it is convenient to explicitly introduce the amplitude and phase of the order parameter $\psi=|\psi|\exp(i\chi)$ and solve the problem by perturbation theory methods: $|\psi|=\psi_0+\psi_1+\psi_2+\ldots$, $\chi=\chi_1+\chi_2+\ldots$, where ψ_j and χ_j ($j=0,1,2,\ldots$) are proportional to the small parameter $\left[cE_0R/(\Phi_0\omega)\right]^j$. We also introduce the dimensionless parameter $\beta=\left(1+\psi_0^2\Gamma^{-2}\right)^{-1/2}$, which is $\beta=1$ in the limiting case of gapless superconductivity and is $\beta\approx\Gamma\psi_0^{-1}\ll 1$ in the low-temperature limit. Then, in the first order of the perturbation theory, Eq. (3) for ψ_1 and χ_1 takes the form

$$\beta\psi_0(iu-\gamma)\chi_{1t}+\beta^{-1}(u+i\gamma)\psi_{1t}$$
$$-\xi_0^2\alpha_0\nabla^2\psi_1-i\xi_0^2\alpha_0\psi_0\nabla^2\chi_1+2\alpha_0\varepsilon\psi_1=0. \quad (4)$$

We assume that the boundary conditions for the order parameter coincide with the boundary conditions of the time-independent Ginzburg–Landau theory:

$$\left.\frac{\partial\psi_1}{\partial r}\right|_{r=R} = 0; \quad \left.\left(\frac{\partial\chi_1}{\partial r} + \frac{2\pi}{\Phi_0}\mathbf{A}_r\right)\right|_{r=R} = 0. \tag{5}$$

Considering harmonic processes, we introduce complex amplitudes $\tilde{p}$ corresponding to quantities p (any of the quantities ψ_1, χ_1, and **A**) as follows:

$$p(r,\theta,t) = \mathrm{Re}\left[\tilde{p}(r,\omega)e^{i\theta - i\omega t}\right]. \tag{6}$$

Since the system is cylindrically symmetric, we look for a solution of Eq. (4) in the form

$$\tilde{\psi}_1 = \tilde{\psi}_{1q}J_1(qr), \quad \tilde{\chi}_1 = \tilde{\chi}_{1q}J_1(qr), \tag{7}$$

where $J_1(x)$ is the first-order Bessel function. Substituting Eqs. (7) into Eq. (4) and separating the real and imaginary parts, we obtain a system of algebraic equations:

$$\begin{cases} i\omega\beta\nu\tilde{\chi}_{1q} - i\omega\tau\beta^{-1}\tilde{\psi}_{1q} + \xi^2q^2\tilde{\psi}_{1q} + 2\tilde{\psi}_{1q} = 0, \\ i\omega\tau\beta\tilde{\chi}_{1q} + i\omega\nu\beta^{-1}\tilde{\psi}_{1q} - \xi^2q^2\tilde{\chi}_{1q} = 0, \end{cases} \tag{8}$$

where $\tau = \tau_0/\varepsilon$ and $\nu = \gamma/(\alpha_0\varepsilon)$. The admissible wavenumbers q included in Eq. (7) are determined by the characteristic equation of the system (8) and have the form (in the derivation, we neglect the terms on the order of ν^2)

$$q_1 = \xi^{-1}\sqrt{i\omega\tau\beta^{-1} - 2}, \quad q_2 = \xi^{-1}\sqrt{i\omega\tau\beta}. \tag{9}$$

It should be noted that the vector potential **A** appears only in the boundary conditions (5), inducing oscillations of the phase of the order parameter. Further, because of electron–hole asymmetry, these phase oscillations excite oscillations of the magnitude of the order parameter with the amplitude proportional to E_0. The characteristic spatial scale of the phase variation is determined only by the wave vector q_2 ($l_\omega = 1/|q_2|$), while the scale of the perturbation of the magnitude of the order parameter is determined by both vectors q_1 and q_2. Taking into account the boundary conditions, the spatial profiles of the magnitude and phase of the order parameter take the form

$$\tilde{\chi}_1 = \frac{2\pi icE_0}{\Phi_0\omega}\frac{J_1(q_2r)}{q_2J_1'(q_2R)}, \tag{10}$$

$$\tilde{\psi}_1 = \frac{2\psi_0\pi cE_0\nu\beta R}{\Phi_0[2 + i\omega\tau(\beta - \beta^{-1})]}\left[\frac{J_1(q_2r)}{q_2J_1'(q_2R)} - \frac{J_1(q_1r)}{q_1J_1'(q_1R)}\right]. \tag{11}$$

Expressions (10) and (11) allow the calculation of the time-averaged magnetic moment M of the disk and the time-averaged azimuthal superconducting current component $\langle j_{s\theta}\rangle$:

$$M = \frac{L}{c}\int_0^R \langle j_{s\theta}\rangle\pi r^2 dr, \tag{12}$$

where

$$\langle j_{s\theta}(r)\rangle = \frac{4\pi\alpha_0T_c\xi_0^2c}{\Phi_0}\psi_0^2\mathrm{Re}\left[\tilde{\psi}_1\left(\frac{i\tilde{\chi}_1^*}{r} - \frac{2\pi}{\Phi_0}\tilde{A}_\theta^*\right)\right]. \tag{13}$$

Substituting the expressions for $\tilde{\psi}_1$ and $\tilde{\chi}_1$ into Eq. (13) and integrating over the radial coordinate in Eq. (12), we finally obtain the time-independent component of the magnetic moment in the form

$$M = G\frac{\gamma\beta R^4}{\omega}\mathrm{Re}\left[\frac{2F}{2 + i\omega\tau(\beta - \beta^{-1})}\right], \tag{14}$$

where $G = 8\pi^4\xi_0^2c^2LE_0^2\alpha_0/(b\Phi_0^3)$ and

$$F = \frac{2(x_1^2f(x_2^*) - x_2^{*2}f(x_1))}{x_1^2(x_1^2 - x_2^{*2})} - \frac{f(x_2^*) + f(x_2)}{x_2^2}. \tag{15}$$

Here, $x_1 = q_1R$, $x_2 = q_2R$, and $f(x) = J_2(x)/J_1'(x)$, where $J_n(x)$ is the nth-order Bessel function and the prime stands for the first derivative. We note that $|x_1| > |x_2|$ and $x_2^2 = -x_2^{*2}$ at any valid parameters.

The form of the temperature and frequency dependences of the calculated magnetic moment M is determined by the relation between four key parameters: radiation frequency ω, renormalized inverse Ginzburg–Landau time $\omega_{GL} = \beta\tau^{-1}$, and two inverse times $\omega_\Delta = \beta\tau_T^{-1}$ and $\omega_\chi = \beta^{-1}\tau_T^{-1}$, where $\tau_T = \tau_0(R/\xi_0)^2$ is the Thouless time for a disk.

To illustrate the mechanism responsible for the appearance of a maximum on the dependences $M(T)$ at a fixed frequency, we first consider the case of large disks, for which $R \gg \xi_0(\Delta_0/\Gamma)$. In this case, perturbations of the magnitude of the order parameter and of the electrochemical potential caused by the derivative $\partial\chi/\partial t$ are localized near the edge of the disk, and the spatial decay scale of ψ_1 determined by the wavenumber q_1 in Eq. (9) depends on the ratio between the radiation frequency ω and the ω_{GL} value. At a fixed frequency in the high-frequency region, where $\omega \gg \omega_{GL}$, the wavenumber q_1 depends on T only through the weak dependence $\beta(T)$, so that, as the temperature decreases, the magnetic moment increases as $M \propto \varepsilon$, which corresponds to the temperature dependence of the quantity ψ_0^2. At a further decrease in the temperature, the frequency ω becomes less than ω_{GL}, and the scale of radial decay of perturbations ψ_1 becomes on the order of ξ. In this case, the phase difference between the perturbation of the magnitude of the

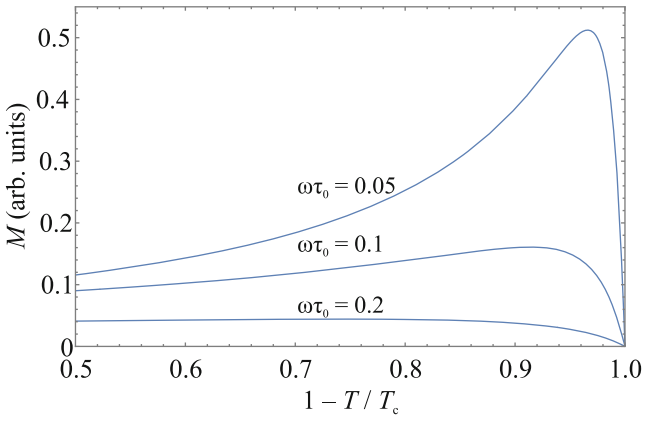

Fig. 2. (Color online) Temperature dependences of the magnetic moment of the disk for different frequencies of the incident circularly polarized wave. The calculation was made for $R = 15\xi_0$ and $\Delta_0 = 5\Gamma$.

order parameter and the azimuthal velocity component tends to $\pi/2$, which, in accordance with Eq. (13), effectively leads to the suppression of the magnetic moment. To describe the crossover between the two described regimes, we take into account that the previously defined function $f(x)$ at large magnitudes of the complex argument may be represented in the form $f(x) = -1 + ix^{-1} - 0.5x^{-2} + O\left(x^{-3}\right)$. The substitution of this function into Eq. (15) and Eq. (15) into Eq. (14) gives the following expression for the magnetic moment (corresponding dependences $M(T)$ are shown in Fig. 2):

$$M = \frac{2G\gamma R^2\xi_0^2}{\omega}\frac{\beta\varepsilon}{4\beta^2\varepsilon^2 + \omega^2\tau_0^2}. \qquad (16)$$

This dependence $M(\varepsilon)$ has a maximum at $2\beta\varepsilon = \omega\tau_0$. The substitution of an explicit expression for β into this condition leads to a quadratic equation for the quantity ε, corresponding to the magnetic moment maximum: $\omega\tau_0\sqrt{1 + \Delta_0^2\varepsilon/\Gamma^2} = 2\varepsilon$. In contrast to the case of gapless superconductors, the frequency dependence of this temperature is nonlinear. The physical reason for the appearance of the maximum is the dephasing between the oscillations of the magnitude and phase of the order parameter with a decrease in the temperature and, correspondingly, in the characteristic relaxation time of perturbations in the superconducting condensate.

Now we analyze the frequency dependence of the magnetic moment at different temperatures. To this end, it is convenient to use the diagrams on the temperature–frequency plane shown in Fig. 3 for disks with different ratios between the radius R and the spatial scale $\xi_0(\Delta_0/\Gamma)$. Regions denoted by Roman numerals correspond to asymptotic regimes with different temperature and frequency dependences of the

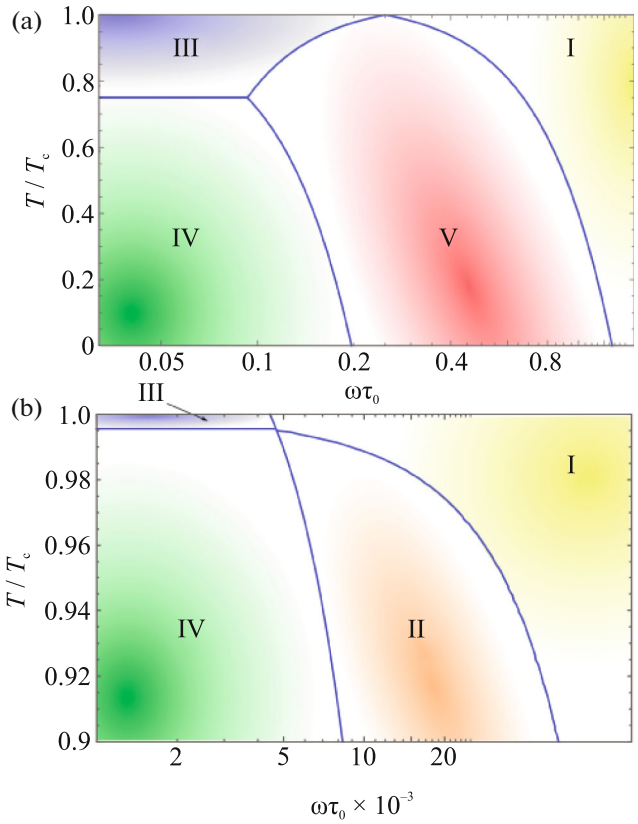

Fig. 3. (Color online) Schematic representation of different ranges of parameters and asymptotic expressions for the magnetic moment obtained with the parameters (a) $\Gamma/\Delta_0 = 0.2$, $R/\xi_0 = 2$ and (b) $\Gamma/\Delta_0 = 0.2$, $R/\xi_0 = 15$. The areas of applicability of various asymptotic expressions for the magnetic moment are schematically marked with color. The I–II and IV–V boundaries; II–IV, I–III, and I–V boundaries; III–IV boundary; and III–V boundary are defined by the relations $\beta\varepsilon = \omega\tau_0$, $R^2\beta\omega\tau_0 = \xi_0^2$, $R^2\varepsilon = \xi_0^2$, and $R^2\omega\tau_0 = \beta\xi_0^2$, respectively.

magnetic moment, and the solid lines indicate the boundaries between regions. In the high-frequency limit, when ω exceeds all other characteristic inverse times ω_{GL}, ω_Δ, and ω_χ (region I), the expression for M takes the form

$$M_I = \frac{2G\gamma R^2\xi_0^2\beta\varepsilon}{\tau_0^2\omega^3}. \qquad (17)$$

In the opposite limiting case, where the radiation frequency is much less than the other characteristic inverse times, the magnetic moment behaves as $M \propto E_0^2\omega$, but the factor in this expression depends on the relation between the radius and the temperature-dependent coherence length ξ: near T_c (at $R \ll \xi$, region III),

$$M_{III} = \frac{73}{5760}\frac{G\gamma R^{10}\beta\varepsilon\omega\tau_0^2}{\xi_0^6}, \qquad (18)$$

while at lower temperatures, where $R \gg \xi$ (region IV),

$$M_{\mathrm{IV}} = \frac{7}{192}\frac{G\gamma R^6 \beta\omega\tau_0^2}{\xi_0^2\varepsilon}. \quad (19)$$

Note that the behavior of the magnetic moment in the high- and low-frequency limits qualitatively coincides with the behavior of M in the case of gapless superconductors. At the same time, there are significant differences between these two cases in the region of intermediate frequencies. The main one is the existence of two different frequency scales ω_Δ and ω_χ, which coincide with each other in the zero gap limit. The difference between these scales leads to the existence of region V in the diagram for $R \ll \xi_0(\Delta_0/\Gamma)$ (Fig. 3a), which is absent for gapless superconductors and in which

$$M_{\mathrm{V}} = \frac{7}{48}\frac{G\gamma R^6 \beta^3\varepsilon}{\xi_0^2\omega}. \quad (20)$$

The boundaries of this region are determined by the condition $\omega_\Delta \ll \omega \ll \omega_\chi$ for the case $R \ll \xi$ and the condition $\omega_{\mathrm{GL}} \ll \omega \ll \omega_\chi$ for the case $R \gg \xi$. In the case of large-radius disks, for which $R \gg \xi_0(\Delta_0/\Gamma)$ (Fig. 3b), the intermediate frequency region (region II) is limited to the frequency interval $\omega_\chi \ll \omega \ll \omega_{\mathrm{GL}}$ and exists only at $R \gg \xi$. The magnetic moment in this region is described by Eq. (16).

It should be noted that, in contrast to the case of gapless superconductors, the boundary between regions I and II, at which the magnetic moment reaches its maximum as a function of the temperature, is nonlinear, which shifts the maximum to lower temperatures. This circumstance should facilitate a more accurate experimental detection of the maximum, since it corresponds to the temperature range of well-developed superconductivity. A similar maximum on dependences $M(\varepsilon)$ is observed also at the transition from regions III to regions IV for disks of an arbitrary radius.

For the experimental observation of the inverse Faraday effect, it seems optimal to use high-temperature cuprates or iron-based superconductors. Their advantage is due to the relatively large value Δ/E_{F} (and, accordingly, a large γ value) and low values of the density of states, which result in a smaller depolarization-induced suppression of the field. Using the parameters $T_{\mathrm{c}} \sim 100$ K and $\tau_{\mathrm{ph}} \sim 10^{-12}$ s [41, 42], we obtain the characteristic values $\tau_0 \sim 2\times10^{-14}$ s and $\Gamma/\Delta_0 \sim 0.01$. Within our model, the electron–phonon relaxation time τ_{ph} limits the radiation frequency $\omega \lesssim \tau_{\mathrm{ph}}^{-1}$. At such frequencies, the maximum on the dependence $M(T)$ is determined by the condition $\beta\varepsilon = \omega\tau_0/2$, which is reached at temperatures $T \sim T_{\mathrm{c}}\left(1-\omega^2/\omega_c^2\right)$, where $\omega_c \sim \tau_0\Delta_0/\Gamma \sim 10^{12}$ s^{-1}. An alternative method for detecting the inverse Faraday effect is based on the nonequilibrium excitation and subsequent detection of vortices of different polarities generated by the Kibble–Zurek mechanism (see [43] and references therein). In this case, the dynamics of vortices after rapid cooling of the sample leads to the preferential exit of vortices of a certain polarity from the disk. One of the key parameters that determine the final difference in the number of vortices having opposite polarity is the localization scale of the superconducting current near the edge of the disk, which is determined by the quantity l_ω. This value is much larger in the Kramer–Watts-Tobin model than in the gapless superconductivity model, which should lead to more efficient generation of nonzero disk vorticity.

Thus, we have shown that the temperature dependences of the magnetic moment of the disk have a maximum in a wide range of system parameters. The maximum for disks of a sufficiently large radius $R \gg \xi_0\Delta_0/\Gamma$ in the limit of high frequencies (at $\omega \gg \tau_T^{-1}$) is reached at temperatures determined by the condition $\omega_{\mathrm{GL}} \sim \omega/2$, while the position of the maximum in the opposite limiting case (at $\omega \ll \tau_T^{-1}$) is determined by the condition $\xi \sim R$. It has also been shown that the finite superconducting gap in the excitation spectrum for small disks with a radius $R \ll \xi_0\Delta_0/\Gamma$ leads to the appearance of new regimes, which are absent in gapless superconductors. In particular, an additional interval of radiation frequencies arises at $\beta < 1$, where the magnetic moment of the disk depends on the temperature and frequency as $M \sim E_0^2\beta^3\varepsilon/\omega$. In conclusion, we note that the depolarization effects described by Eq. (1) can change the frequency and temperature dependences of the magnetic moment; therefore, the determination of parameters that are optimal for the experimental observation of the predicted effects requires an analysis of the geometry of a particular sample.

FUNDING

This work was supported by the Russian Science Foundation (project no. 21-72-10161). A.S. Mel'nikov acknowledges the support of the Ministry of Science and Higher Education of the Russian Federation (project no. FSMG-2023-0011, state assignment no. 075-03-2022-106 for the Moscow Institute of Physics and Technology).

CONFLICT OF INTEREST

The authors declare that they have no conflicts of interest.

OPEN ACCESS

This article is licensed under a Creative Commons Attribution 4.0 International License, which permits use, sharing, adaptation, distribution and reproduction in any medium or format, as long as you give appropriate credit to the original author(s) and the source, provide a link to the Creative Commons license, and indicate if changes were made. The images or other third party material in this article are included in the article's Creative Commons license, unless indicated otherwise in a credit line to the material. If material is not included in the article's Creative Commons license and your intended use is not permitted by statutory regulation or exceeds the permitted use, you will need to obtain permission directly from the copyright holder. To view a copy of this license, visit http://creativecommons.org/licenses/by/4.0/.

REFERENCES

1. I. Chiorescu, Y. Nakamura, C. J. P. M. Harmans, and J. E. Mooij, Science (Washington, DC, U. S.) **299**, 1869 (2003).
2. S. Anders, M. G. Blamire, F.-I. Buchholz, D.-G. Crété, R. Cristiano, P. Febvre, L. Fritzsch, A. Herr, E. Il'ichev, J. Kohlmann, J. Kunert, H.-G. Meyer, J. Niemeyer, T. Ortlepp, H. Rogalla, et al., Phys. C (Amsterdam, Neth.) **410**, 2079 (2010).
3. M. Eschrig, Adv. Phys. **55**, 47 (2006).
4. J. Linder and J. Robinson, Nat. Phys. **11**, 307 (2015).
5. S. Mironov, E. Goldobin, D. Koelle, R. Kleiner, Ph. Tamarat, B. Lounis, and A. Buzdin, Phys. Rev. B **96**, 214515 (2017).
6. W. Magrini, S. V. Mironov, A. Rochet, P. Tamarat, A. I. Buzdin, and B. Lounis, Appl. Phys. Lett. **114**, 142601 (2019).
7. S. Mironov, H. Meng, and A. Buzdin, Appl. Phys. Lett. **116**, 162601 (2020).
8. S. V. Mironov and A. I. Buzdin, Phys. Rev. B **104**, 134502 (2021).
9. G. M. Eliashberg, JETP Lett. **11**, 114 (1970).
10. T. M. Klapwijk, J. N. van den Bergh, and J. E. Mooij, J. Low Temp. Phys. **26**, 385 (1977).
11. D. Fausti, R. I. Tobey, N. Dean, S. Kaiser, A. Dienst, M. C. Hoffmann, S. Pyon, T. Takayama, H. Takagi, and A. Cavalleri, Science (Washington, DC, U. S.) **331**, 189 (2011).
12. R. Mankowsky, A. Subedi, M. Först, et al., Nature (London, U.K.) **516**, 71 (2014).
13. S. Veshchunov, W. Magrini, S. V. Mironov, A. G. Godin, J.-B. Trebbia, A. I. Buzdin, Ph. Tamarat, and B. Lounis, Nat. Commun. **7**, 12801 (2016).
14. S. V. Mironov, A. S. Mel'nikov, I. D. Tokman, V. Vadimov, B. Lounis, and A. I. Buzdin, Phys. Rev. Lett. **126**, 137002 (2021).
15. M. D. Croitoru, B. Lounis, and A. I. Buzdin, Phys. Rev. B **105**, L020504 (2022).
16. M. D. Croitoru, S. V. Mironov, B. Lounis, and A. I. Buzdin, Adv. Quantum Technol. **5**, 2200054 (2022).
17. V. D. Plastovets, I. D. Tokman, B. Lounis, A. S. Mel'nikov, and A. I. Buzdin, Phys. Rev. B **106**, 174504 (2022).
18. L. P. Pitaevskii, Sov. Phys. JETP **12**, 1008 (1961).
19. J. P. van der Ziel, P. S. Pershan, and L. D. Malmstrom, Phys. Rev. Lett. **15**, 190 (1965).
20. A. Kirilyuk, A. V. Kimel, and T. Rasing, Rev. Mod. Phys. **82**, 2731 (2010).
21. A. Kirilyuk, A. V. Kimel, and T. Rasing, Rep. Prog. Phys. **76**, 026501 (2013).
22. V. Kimel, A. Kirilyuk, P. A. Usachev, R. V. Pisarev, A. M. Balbashov, and Th. Rasing, Nature (London, U.K.) **435**, 655 (2005).
23. C. D. Stanciu, F. Hansteen, A. V. Kimel, A. Tsukamoto, A. Itoh, A. Kirilyuk, and Th. Rasing, Phys. Rev. Lett. **98**, 207401 (2007).
24. O. H.-C. Cheng, D. H. Son, and M. Sheldon, Nat. Photon. **14**, 365 (2020).
25. R. Hertel, J. Magn. Magn. Mater. **303**, L1 (2006).
26. R. Hertel and M. Fähnle, Phys. Rev. B **91**, 020411(R) (2015).
27. M. Battiato, G. Barbalinardo, and P. M. Oppeneer, Phys. Rev. B **89**, 014413 (2014).
28. I. D. Tokman, Phys. Lett. A **252**, 83 (1999).
29. G. F. Quinteiro and P. I. Tamborenea, Europhys. Lett. **85**, 47001 (2009).
30. K. L. Koshelev, V. Yu. Kachorovskii, and M. Titov, Phys. Rev. B **92**, 235426 (2015).
31. K. L. Koshelev, V. Yu. Kachorovskii, M. Titov, and M. S. Shur, Phys. Rev. B **95**, 035418 (2017).
32. O. V. Kibis, Phys. Rev. Lett. **107**, 106802 (2011).
33. M. V. Durnev and S. A. Tarasenko, Phys. Rev. B **103**, 165411 (2021).
34. L. Kramer and R. J. Watts-Tobin, Phys. Rev. Lett. **40**, 1041 (1978).
35. R. J. Watts-Tobin, Y. Krähenbühl, and L. Kramer, J. Low Temp. Phys. **42**, 459 (1981).
36. A. A. Golub, Sov. Phys. JETP **44**, 178 (1976).
37. G. Shon and V. Ambegaokar, Phys. Rev. B **19**, 3515 (1979).
38. B. I. Ivlev and N. B. Kopnin, Sov. Phys. Usp. **27**, 206 (1984).
39. L. D. Landau, L. P. Pitaevskii, and E. M. Lifshitz, *Course of Theoretical Physics,* Vol. 8: *Electrodynamics of Continuous Media* (Pergamon, New York, 1984; Fizmatlit, Moscow, 2001).
40. N. B. Kopnin, *Theory of Nonequilibrium Superconductivity* (Oxford Science, London, 2001).
41. S. G. Doettinger, S. Kittelberger, R. P. Huebener, and C. C. Tsuei, Phys. Rev. B **56**, 14157 (1997).
42. A. Pashkin, M. Porer, M. Beyer, K. W. Kim, A. Dubroka, C. Bernhard, X. Yao, Y. Dagan, R. Hackl, A. Erb, J. Demsar, R. Huber, and A. Leitenstorfer, Phys. Rev. Lett. **105**, 167001 (2010).
43. V. D. Plastovets, I. D. Tokman, B. Lounis, A. S. Mel'nikov, and A. I. Buzdin, Phys. Rev. B **106**, 174504 (2022).

Translated by L. Mosina